AD-A082 727 MASSACHUSETTS INST OF TECH LEXINGTON LINCOLN LAB F/G 17/9
IRAR IMAGE PROCESSING TECHNIQUES.(U)
NOV 79 D R SULLIVAN F19628-80-C-0002
UNCLASSIFIED TST-41 ESD-TR-79-271 NL

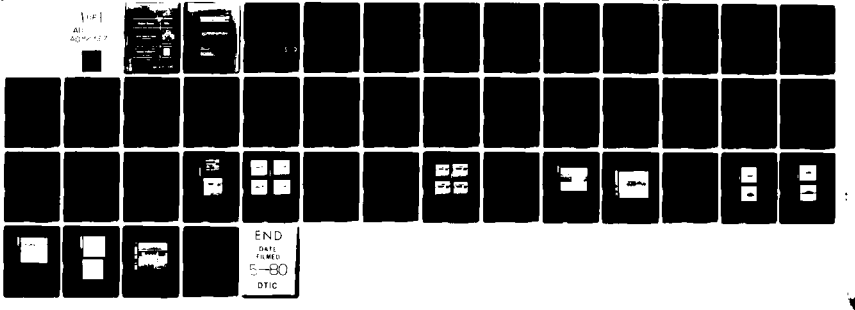

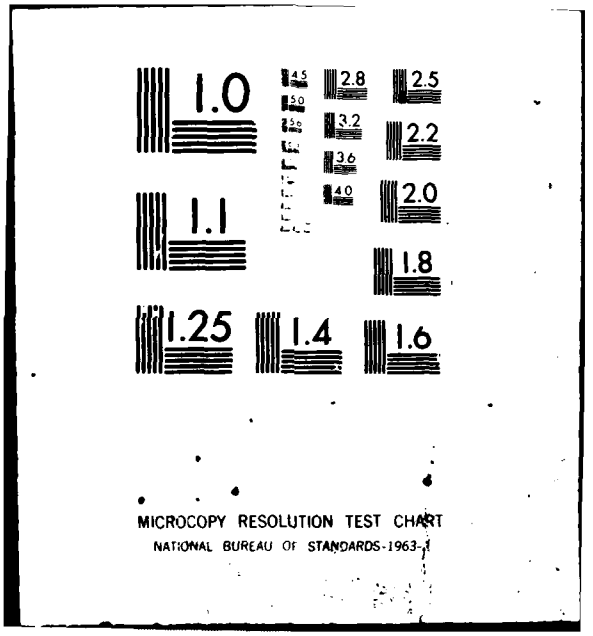
1.0
1.1
1.25
1.4
1.6
1.8
2.0
2.2
2.5
2.8
3.2
3.6
4.0
4.5
5.0
5.6
MICROCOPY RESOLUTION TEST CHART
NATIONAL BUREAU OF STANDARDS-1963-A

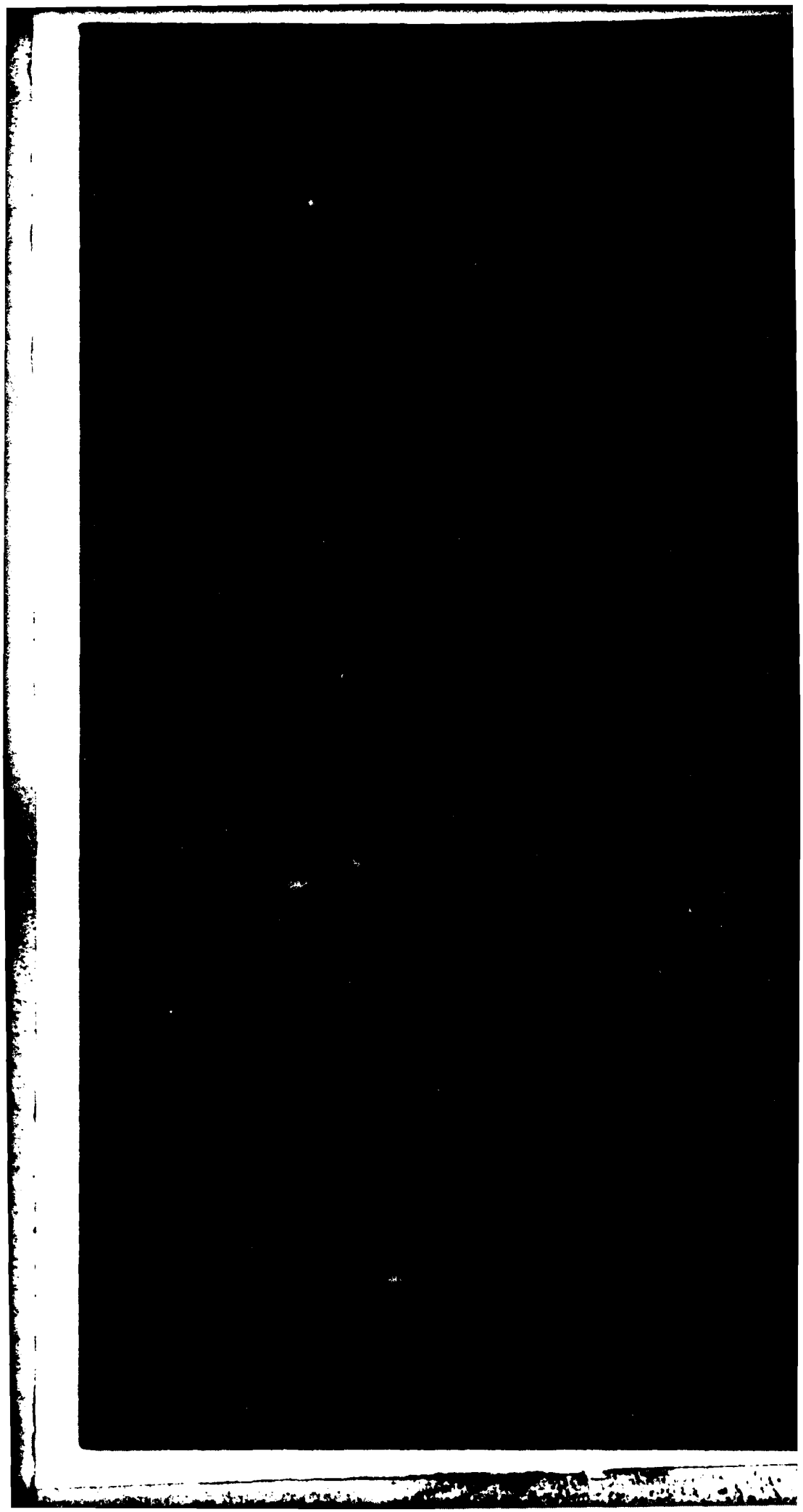

MASSACHUSETTS INSTITUTE OF TECHNOLOGY

LINCOLN LABORATORY

# IRAR IMAGE PROCESSING TECHNIQUES

*D. R. SULLIVAN*

*Group 53*

PROJECT REPORT TST-41
(Tactical Systems and Technology)

7 NOVEMBER 1979





LEXINGTON MASSACHUSETTS

## ABSTRACT

This report examines the problems associated with the display of active (10.6μm) infrared radar images. Issues addressed include degradations introduced by the imaging sensor, the effects of these degradations on image tracking and image enhancement, and evaluation of various tracking and enhancement techniques in view of their usefulness and potential hardware implementation. The performance of each algorithm is demonstrated using either simulated data or data collected by the Infrared Airborne Radar (IRAR) testbed system.

CONTENTS

## LIST OF ILLUSTRATIONS

LIST OF ILLUSTRATIONS (cont)

# 1. INTRODUCTION

The Infrared Airborne Radar (IRAR) program was initiated to develop the technology required for an imaging and moving target indicator (MTI) infrared radar for tactical applications. When operated in a continuous wave form (CW) mode, the radar would provide wide field search and automatic detection of moving targets. When the laser is switched to pulsed operation, the system provides a high resolution image. The planned data rate of thirty frames per second permits signal averaging within a time frame compatible within mission requirements. Further description of the applications and overall system requirements are given by R. J. Becherer[1].

Image processing techniques are being investigated to reduce degrading effects present in infrared active imagery and for the purpose of image enhancement. Image quality is severely limited by speckle, which arises from the coherent nature of the illuminating laser beam and the surface roughness of most targets (see, for example, J. C. Dainty[2] for a more complete description of speckle). Techniques that have been developed to minimize the effect of speckle and improve image quality are presented. A procedure to provide a three-dimensional quality to images when range information is available is also described. Finally, conclusions concerning the utility and adaptability of these image processing techniques are presented.

## 1.1 Data Recording Format and Playback Facility

The IRAR testbed system provides digital recording of the intensities of a 128 by 128 array of picture elements (pixels). The intensities I(i, j),

for $1 \leq i, j \leq 128$, are proportional to the strengths of the return of the associated laser pulse within a pre-set range gate. The range, R(i, j), at which the peak intensity of each pixel is detected is also recorded. These digital tapes are processed on Lincoln Laboratory's time-shared computer which is interfaced through a minicomputer to a graphic display system. All the imagery presented in this report was generated by the testbed system and photographed from the graphic display device. Details of the radar system including the signal processor are given by Hull and Marcus[3].

## 1.2 Processing Considerations

In an attempt to present a subjectively more pleasing and more easily recognizable image to an observer, IRAR data have been processed using various enhancement techniques. Certain known degradations present in an IRAR image were taken into consideration during the selection of algorithms. The coherence of the IRAR illumination source produces a non-linear intensity effect called speckle such that samples reflected from a uniform diffuse surface, I(i, j), are Rayleigh power (exponentially) distributed about the mean reflectance. A second problem arises when the laser beam is normal to the tangent of a curved metallic surface. The amplitude of this return is typically orders of magnitude greater than a return from a diffuse target. These usually saturated returns, called glints, and the degradations due to speckle present particularly difficult problems in terms of image tracking and image display. Small motions of the target or sensor can give a target large 'apparent' frame-to-frame motion as the position of each glint (off the target) either drastically changes or disappears. In terms of speckle,

motion will change the observed intensity of each pixel across the target from frame-to-frame. Therefore, the detection of target motion is a problem to be addressed. Also both speckle and glints are undesirable in a displayed image. With this phenomenology in mind, many algorithms were tried in software to test their feasibility for a future IRAR system.

## 2. IMAGE PROCESSING TECHNIQUES

### 2.1 Frame Averaging

A visible photograph taken with a telephoto lens (Figure 1a) and a single frame of IRAR, intensity-only, data (Figure 1b) demonstrate how speckle introduces a marked intensity variation in the infrared compared to the same scene imaged with noncoherent radiation in the visible. Although speckle limits image quality, motion in an airborne system will provide the spatial decorrelation necessary for frame averaging to effectively minimize this degradation. Because data taken with the stationary testbed system exhibit spatial correlation, the improvement in image quality realized by noncoherent averaging of this type of data is limited. Therefore, to demonstrate the advantages gained by frame averaging, a computer simulation of spatially decorrelated frames was generated.

The computer generated reference image of a Cessna aircraft is presented in Figure 2a. This reference image is then implanted into a gaussian background (not shown) to form an estimate of a 'speckle-free' image. Each pixel in the speckle-free image can be thought of as truly representative of the mean reflectance of that resolution element in the field of view. For each pixel from the speckle-free image, the following process is performed to

simulate speckle. The digital value of each pixel is used as input to a random number generator which produces an exponentially distributed value about the input (i.e., about the mean reflectance). Performing this step for every pixel individually guarantees spatial and temporal decorrelation.

The image quality of a single, intensity-only, simulation frame (Figure 2b) is significantly improved when frame averaging is used as is shown in Figures 2c and 2d. The improvement in the signal-to-noise ratio is equal to the square root of the number of frames averaged. The visual improvement gained by averaging four to eight frames seems to be sufficient for target recognition. Temporal frame averaging not only compensates for speckle and, to some extent glints, but it also reduces the effects of other randomly distributed, zero mean noise components. In light of these advantages, frame averaging of intensity data has been the most consistently useful algorithm applied to IRAR data.

The expression for frame averaging L intensity-only frames of data is

$$f(i, j) = \frac{1}{L} \sum_{k=1}^{L} f_k(i + \Delta i, j + \Delta j) \qquad \begin{matrix} 1 \leq i \leq x \\ 1 \leq j \leq y \end{matrix} \qquad (1)$$

for an x row by y column image matrix where $\Delta i$, $\Delta j$ account for frame-to-frame motion. The process of registering consecutive data frames so that frame averaging can be performed without image blur is the primary problem in implementing this technique.

## 2.2 Image Tracking

Two classes of tracking algorithms have been investigated for the purpose of image registration. Both classes assume that the area of interest be

initially supplied by a cueing technique. This location will be used as the center point of a tracking window which will move in subsequent frames so that it always contains the designated target.

The first class of algorithms, centroid trackers, calculate the 'center of mass' or the positionally weighted average of the intensities of points within the track window. The mean intensity of the M by N tracking window, $\mu_{tf}$, can be expressed as

$$\mu_{tf} = \frac{1}{MN} \sum_{i=1}^{M} \sum_{j=1}^{N} f(i, j) \tag{2}$$

The positionally weighted row centroid can be defined as

$$i_c = \frac{\sum_{i=1}^{M} \sum_{j=1}^{N} i(f(i, j) - \mu_{tf})}{\sum_{i=1}^{M} \sum_{j=1}^{N} (f(i, j) - \mu_{tf})} \tag{3}$$

and the column centroid can be defined as

$$j_c = \frac{\sum_{i=1}^{M} \sum_{j=1}^{N} j(f(i, j) - \mu_{tf})}{\sum_{i=1}^{M} \sum_{j=1}^{N} (f(i, j) - \mu_{tf})} \tag{4}$$

Therefore the window coordinates $(i_c, j_c)$ point to the location of the centroid. The pseudo-centroid tracker reduces the above expression to a binary calculation through the following transformation

$$f'(i, j) = \begin{cases} 1 & , \text{if } f(i, j) - \mu_f > 0 \\ 0 & , \text{otherwise} \end{cases} \tag{5}$$

In this case, the mean intensity of the entire image, $\mu_f$, is used to suppress the background which often has a lower mean intensity than the mean of the target. Clearly, some other suitably chosen threshold could be used instead of the global mean.

The predicted performance of the centroid tracker as defined by Kingston and Gruber has been confirmed using computer generated speckled images[4]. An expression for the tracking accuracy associated with locating the centroid is formulated

$$\varepsilon_i = \frac{1}{12} \frac{\sigma_{tf}}{\mu_{tf}} \sqrt{\frac{M}{N}}, \quad \varepsilon_j = \frac{1}{12} \frac{\sigma_{tf}}{\mu_{tf}} \sqrt{\frac{N}{M}} \tag{6}$$

where $\mu_{tf}$ and $\sigma_{tf}$ are the first and second order statistics of the points in the tracking window. Figure 3 presents some simulation results using a centroid tracker.

The other class of image trackers uses the correlation matrix as a means by which to measure the 'goodness of match' between two consecutive data frames. Because this algorithm class is much less sensitive to any one absolute pixel value than the centroid tracker, it should have superior tracking performance. The normalized cross correlation function yields a value, $\rho$, such that $-1 \leq \rho \leq 1$ and

$$\rho(\Delta i, \Delta j) = \frac{\sum_{i=1}^{M} \sum_{j=1}^{N} (f(i, j) - \mu_{tf})(g(i + \Delta i, j + \Delta j) - \mu_{tg})}{(\sigma_{tf}\, \sigma_{tg})/MN} \tag{7}$$

where f and g are two consecutive intensity frames of data separated in time

by $\Delta T$. The terms $\Delta i$, $\Delta j$ symbolically indicate that g is shifted with respect to f. For each shifted position, f is convolved with g and properly normalized so that a new value of $\rho$ is calculated. The matrix of correlation coefficients is searched to find the peak value, $\rho'$,

$$\rho' = \max |\rho| \tag{8}$$

This is considered to be the most likely place for a match. The position of $\rho'$ in the matrix of correlation coefficients determines the motion between the two data frames, f and g. Using interpolation techniques, f and g can be registered to within a fraction of a pixel.

The expected theoretical performance of a one-dimensional correlation tracker has the following form

$$\varepsilon = \left( \frac{(\sigma_t/\mu_t)^4 \, (M - 1) + 2 \, (\sigma_t/\mu_t)^2}{8} \right)^{1/2} \tag{9}$$

where $\mu_t$, $\sigma_t$ denotes the first and second order statistics of the target within the tracking window and M equals the extent of the target in pixels. A computer generated speckled signal is used to evaluate the predicted accuracy, $\varepsilon$, of a correlation tracker. A comparison of these simulated signals and their theoretical counterpart can be found in Figure 4.

Although the results presented in Figures 3 and 4 seem to indicate that centroid tracking should provide more accurate tracking information, it should be noted that these simulations (and also (6) and (9)) assume purely diffuse targets, without glints. Because centroid trackers are particularly sensitive to large, single point variations characteristic of glints, it is

felt that the accuracy of a centroid tracker under more realistic conditions will be degraded. Secondly, it has been experimentally verified that a target can reflect most of the transmitted power incident on its surface away from the receiver. Consequently, the silhouette of the target, contrast reversed, can suddenly appear in the tracking window as the aspect angle between sensor and target changes. It is evident that in equations (3) and (4) the position of the centroid over a tracking window containing a contrast reversed target is a function of the clutter rather than the target. Cross correlation of a contrast reversed target and its positive complement yields a peak correlation coefficient approximately equal in magnitude to the cross correlation of two similar images (e.g., two "positive" images), but opposite in sign. Under these conditions a centroid tracker would most likely fail, while a correlation tracker would maintain track.

Qualitatively, the correlation tracker has yielded the best results. However, implementing a correlation tracker using either (7) or using the corresponding FFT algorithm is computationally expensive with respect to time. Efforts are underway either to find other algorithms that perform as well but are more feasible in terms of IRAR's frame rate, or to devise more economical methods to implement the correlation tracker.

### 2.3 Low Pass Filtering

The first approach taken to enhance IRAR imagery involves reducing the visually degrading effects due primarily to speckle (Figure 1b). Frame averaging eight intensity-only IRAR images (Figure 5a) helps to reduce this problem by improving the signal-to-noise ratio by $2\sqrt{2}$. There are also

some low pass filtering techniques which compensate for the high frequency artifacts caused by speckle noise and glints. Three low pass filters, specifically a two-dimensional moving average filter, a homomorphic filter, and a two-dimensional median filter, were tested on IRAR data[5, 6, 7].

The moving average filter convolves the two-dimensional mask

$$\frac{1}{9}\begin{vmatrix} 1 & 1 & 1 \\ 1 & 1 & 1 \\ 1 & 1 & 1 \end{vmatrix}$$

with a 3 x 3 pixel area from the matrix, I. Rather than displaying pixel I(i, j), the average value of the local neighborhood of I(i, j) is used. The mask is then shifted over the image until all points in I have been filtered. An example of this filtering technique, where the matrix, I, is an eight frame average of intensity-only data, is shown in Figure 5b.

Homomorphic filtering assumes that noise (i.e.,speckle) is multiplicative in the time domain

$$I(i, j) = S(i, j)\, N(i, j) \qquad (10)$$

Taking the logarithm of both sides of (10) makes the noise term additive to the signal term

$$\log(I(i, j)) = \log(S(i, j)) + \log(N(i, j)) \qquad (11)$$

The fourier transform of this image, which preserves the linear relationship in (11), allows selective de-emphasis of high frequency fourier coefficients.

An inverse transform followed by exponentiation back into the original dynamic range completes the low pass filter process (Figure 5c).

Median filtering is a non-linear 'window' function which operates in the time domain. By examining a neighborhood or window around a central pixel, I(i, j), the digital values within that window are sequentially ordered so that the median value can be extracted and saved in a separate display matrix. The window is then moved until the entire image is filtered. Both the non-separable (two-dimensional neighborhood) and the separable (filtered with respect to rows, then with respect to columns) variations were tried. The major disadvantage of using the non-separable median filter is its tendency to smooth out sharp corners found in man-made objects. For that reason, the separable median filter of dimension three was used on an eight frame average, intensity-only, image shown in Figure 5d.

Comparing the three algorithms, each has both advantages and disadvantages. Homomorphic filtering performed on an eight frame average is presented in Figure 5c. Aside from its computational complexity, the exact form of the transfer function to attenuate high frequencies is a controversial issue[8]. The moving average filter and the median filter are also applied to the frame averaged image. Their comparative simplicity make these filters attractive in terms of execution time. The moving average filter, although easy to implement, has two major drawbacks. The relatively large single point digital spikes characteristic of glints are merely attenuated. Also, this filter tends to blur edges. The median filter has many desirable properties including ease of implementation and the ability to eliminate rather than

attenuate the noise spikes characteristic of glints. Although median filtering will tend to give an image a block-like appearance, there are interpolative techniques which can be employed to correct for this artifact.

## 2.4 Contrast Manipulation

The IRAR data recording format defines the data dynamic range as eight bits or 256 discrete values. When displaying IRAR data, a transformation into the display dynamic range must be made. Although low pass filtering reduces noise, it does not alter image contrast which may be poor in terms of the human visual system. Consequently, various contrast manipulation techniques have been investigated in order to present a more visually pleasing displayed image.

Histogram modification uses statistical parameters associated with an image matrix to define the display of that image[9, 10]. By tabulating the discrete probability density function (histogram) of the intensities within the input image, I, a transformation from this histogram into a chosen output density function can be made. Figure 6 demonstrates histogram equalization which defines the output distribution as uniform, mapping the input distribution into N approximately equiprobable bins. A slight variation of this algorithm, using an adaptive threshold to suppress low intensity background samples combined with exponential rescaling, was developed specifically for use on IRAR data. The threshold, T, is defined as

$$T = M + k\,\sigma_f \qquad \text{for} \qquad .25 \leq k \leq .75 \qquad (12)$$

where M is the most frequently occurring digital count in the histogram, $\sigma_f$ is the standard deviation associated with the samples in the histogram, and k is an empirically determined constant. For all points in the input histogram that exceed T, histogram equalization is performed. Those values less than T are mapped into the darkest level on the display device. Therefore, the dynamic range of the display device is used only to enhance those points greater than T, thereby increasing target contrast.

It has been suggested that these N equiprobable bins be linearly assigned to display output levels. However, linear rescaling does not compensate for the approximately logarithmic response of the eye to display brightness. Consequently, an exponential assignment of equiprobable bins into the display dynamic range was used to linearize, in terms of the human visual system, the displayed output. Examples of this histogram modification technique, applied after frame averaging, are shown in Figure 7 and Figure 8 using pseudocolor which will be described in a subsequent section.

An assumption made in this implementation of histogram modification is that the target of interest is generally greater in intensity than the background and noise. However, as was pointed out in the section on image tracking, contrast reversal can occur depending on the aspect angle of the target with respect to the sensor and the target type. Also, if one considers IRAR as a terrain or obstacle avoidance radar, 'targets' such as wires which have a relatively low mean intensity, may be below the threshold used in histogram modification.

Consequently, a contrast enhancement scheme, which adaptively calculates

an intensity gain constant used to control relative display contrast was developed. Again, using the image histogram, a threshold, A', which is less stringent than the threshold used in histogram modification, scales the lowest intensity returns to a fixed value, A, on the display brightness scale. By calculating the centroid, C', of the bins above the threshold, a gain coefficient, K, can be calculated. Referring to Figure 9, the visually linear portion of the display range between A and B will be the only digital display values used. By calculating K such that C' is mapped into C, that is

$$K = (C-A) \; / \; (C'-A') \qquad (13)$$

the perceived brightness of the image will be visually linear. K is used as a multiplicative gain variable such that for a given input intensity matrix, I, the displayed output matrix, O, will have the following form

$$O(i, j) = \begin{cases} A & , \text{if } (I(i, j) \times K) \leq A \\ B & , \text{if } (I(i, j) \times K) \geq B \\ I(i, j) \times K & , \text{otherwise} \end{cases} \qquad (14)$$

This automatic gain control technique maps target and clutter into the perceptually linear portion of the display brightness scale, maps noise to one level, A, and compresses points most likely to be glints into one level, B. Although the noise will be enhanced as is evident in Figures 10 and 11, low intensity detail has also been enhanced. The low intensity targets, whose intensity returns are not randomly spaced, are now visible.

Histogram modification and automatic gain control show potential for

improvement and use in conjunction with other processing techniques*. They are both computationally compact and efficient as well as effective enhancement tools and are therefore candidates for future consideration.

## 2.5 Edge Detection

As was mentioned earlier, the large, flat metallic surfaces of targets such as trucks may be angled in such a way that the incident radar energy will be specularly reflected away from the receiver causing contrast reversal. In an attempt to deal with this occurrence, several edge detection algorithms were implemented[11,12,13]. Operating with discrete intensity gradients, a target is outlined regardless of its orientation with respect to the sensor. Although many edge detection algorithms were tried, all except one were eventually discarded due to their inability to adaptively compensate for noise found in IRAR imagery.

Robinson[13] presents a comprehensive and adaptive edge detection algorithm which was slightly modified before being applied to IRAR data. In order to determine if the point I(i, j) is an edge point, a three by three neighborhood of I(i, j) is examined in the following way. Given that there are eight discrete edge directions within this neighborhood, the maximum gradient G(i, j) is found by convolving the points from the neighborhood with the matrix

*See subsequent section (2.7) entitled "Range/Intensity Color Mapping".

$$\frac{1}{3}\begin{vmatrix} -1 & -2 & -1 \\ 0 & 0 & 0 \\ 1 & 2 & 1 \end{vmatrix} \qquad (15)$$

Edge Magnitude Mask

and seven rotations of this matrix to account for all eight possible edge directions. Having found the maximum gradient, G(i, j), and its corresponding edge direction, D(i, j) where $0 \leq D(i, j) \leq 7$, G(i, j) is compared to the low pass filtered output, L(i, j), from the convolution of the same neighborhood with the following low pass filter[14]

$$\frac{1}{16}\begin{vmatrix} 1 & 2 & 1 \\ 2 & 4 & 2 \\ 1 & 2 & 1 \end{vmatrix} \qquad (16)$$

G(i, j) is compared to L(i, j) so that

$$G'(i, j) = \begin{cases} G(i, j) & \text{, if } G(i, j) > L(i, j) \\ 0 & \text{, otherwise} \end{cases} \qquad (17)$$

where G'(i, j) = 0 indicates that although a maximum gradient value exists, its magnitude is small and therefore not a major edge.

After the process above is carried out for all points in the matrix, I, the two matrices generated, namely G' and D, are examined to make the final edge determination. If G'(i, j) is non-zero, its three by three neighborhood is inspected to determine if there are at least three non-zero points. If there are fewer than three non-zero values, the corresponding pixel in

the display matrix, O(i, j) is set to zero. Otherwise, the corresponding three by three neighborhood of the edge direction map, D, is examined to determine if the locally preferred edge direction is roughly the same as the edge direction of the center pixel, D(i, j). Each of the eight directions is assigned an integer value between 0 and 7 so that 'roughly the same' really means equal to the value of D(i, j), one less than D(i, j) or one greater than D(i, j), modulo seven. Therefore, the display matrix O has the following form

$$O(i, j) = \begin{cases} N & \text{, if } G'(i,j) \neq 0 \text{ and if } B[D(i,j)] \text{ contains } \geq 6 \\ & \quad \text{values that equal } D(i,j),\ D(i,j)+1, \text{ or } D(i,j)-1 \\ 0 & \text{, otherwise} \end{cases} \qquad (18)$$

where B denotes "the 3 x 3 neighborhood of" and N is the brightness value to be displayed for edge points.

This edge detection algorithm works moderately well at detecting major edges while eliminating most noise and textural edges occurring over the extent of the walls of the flight facility shown in Figure 12. However, the major drawbacks to this algorithm in terms of a portable IRAR system are its storage and time requirements. Also, the input to the edge detector has been preprocessed by frame averaging followed by median filtering. Consequently, this type of processing in an IRAR real-time environment may not be feasible.

## 2.6 Pseudocolor

Using the graphics display device in the color mode rather than in black and white gives an entirely new dimension to image processing.

Pseudocolor, the process by which an arbitrary color assignment is made to each digital value, can by its nature enhance the visual output. Consider, for example, a uniformly reflective square of dimension d x d embedded in a uniform background. Assign a digital value of 100 to the square and 99 to the background. Viewing this scene in black and white makes it impossible to detect the presence of the square whereas a transformation into color using red to display a digital value of 100 and blue to display a digital value of 99 produces a dramatic change (Figure 13). The setup of a useful pseudocolor transformation map, which converts digital value into color on the display device, is no trivial task. Many factors, such as the psychology of the human visual system and display device limitations, play an important role in the choice of a pseudocolor 'video lookup table'. Although the choice of pseudocolor in Figure 8 is not optimum, it demonstrates the potential for use of a pseudocolor image display.

## 2.7 Range/Intensity Color Mapping

Unlike any previously described enhancement technique, range/intensity color mapping utilizes the full capabilities of an optical imaging radar to provide simultaneous range, intensity, and high resolution angular information. A quasi-three-dimensional quality can be imparted to this imagery through the use of a pseudocolor display and the generation of a display matrix, P, which is a function of the input intensity matrix, I, and its corresponding range matrix, R.

The global histogram of I is used to define a noise threshold, T, such that

$$T = M + k\sigma \qquad .1 \leq k \leq .25 \tag{19}$$

where M is the histogram mode, $\sigma$ is the standard deviation of I, and k is an empirically determined constant. The intensity bins greater than T are requantized into a small number, N, of equiprobable bins. Therefore, the intensity mapping is defined as

$$I'(i, j) = \begin{cases} n & , \text{ if } I(i, j) > T \text{ and } 1 \leq n \leq N \\ 0 & , \text{ otherwise} \end{cases} \tag{20}$$

The range matrix, R, is then requantized into a small number, H, bins so that the range mapping has the following form

$$R'(i, j) = \begin{cases} \text{integerpart}[H(R(i,j)-R_{MIN})/(R_{MAX}-R_{MIN})+1], & R_{MIN} \leq R(i,j) < R_{MAX} \\ H & , R(i, j) = R_{MAX} \end{cases} \tag{21}$$

The final mapping, P, into the pseudocolor video lookup table is defined as

$$P(i, j) = \begin{cases} I'(i, j) + (R'(i, j)-1)N & , \text{ for } I'(i, j) \neq 0 \\ 0 & , \text{ otherwise} \end{cases} \tag{22}$$

Consequently, a pixel range value determines the display hue (there are H distinct hues) and the corresponding intensity value, if it passes the threshold T, determines the brightness level of the chosen hue (there are N brightness levels for each hue). Requantizing the range matrix, R, into H visually distinct hues substantially improves the visual appearance by achieving a three-dimensional quality which aids in clutter discrimination. The inclusion of histogram modification in range/intensity color mapping to

encode intensity preserves the relative textural information available in intensity-only imagery. Figure 14 shows an example of range/intensity color mapping using five hues, each hue having six brightness levels*.

## 3. CONCLUSIONS

The single most important processing technique for improving active infrared imagery is frame averaging[17]. Sufficient decorrelation occurs between successive frames either from atmospheric turbulence or relative motion between target and sensor to make significant improvements in the frame averaged imagery. Histogram modification combined with frame averaging improves image contrast and is relatively economical to implement in a real-time processor.

The use of pseudocolor improves general image appearance and enhances low contrast features. When range measurements are available along with the intensity data, range/intensity mapping imparts a three-dimensional quality to the displayed image. Also image 'smoothing' without the loss of edge acuity can be realized because pixels across a target, although varying in brightness, are mapped into the same hue in the range matrix. Color offers sufficient improvement in image quality to warrant serious consideration for tactical systems in spite of its greater cost.

Frame averaging will require an image tracker capable of 1 pixel or better precision. Correlation trackers have been tested which demonstrate

*For a more complete description of this technique, including other photographs, see references 15 and 16.

the required precision. A search is being made for an efficient, rapid implementation of the correlation technique.

This document should be viewed as a progress report rather than a list of processing solutions. Therefore, efforts will continue in the general area of image processing of IRAR data, specifically to make improvements to existing algorithms outlined in this report, and to search for new ideas. Efforts are underway to develop a correlation tracker that will operate in real-time at frame rates up to 15 Hz. Various techniques for speckle reduction on single frame and frame averaged data are being explored[17]. Although a firm decision on an image processing procedure has not been made, the need for processing of infrared radar data is unquestionable and significant improvements in image quality are achievable with the techniques described herein.

## REFERENCES


1. R. J. Becherer, "System Design Study for Infrared Airborne Radar (IRAR)," Technical Note 1977-29, Lincoln Laboratory, M.I.T. (18 October 1977), DDC AD-A048979/9.

2. J. C. Dainty et al., Topics in Applied Physics, Vol. 9 (Springer-Verlag, New York, 1975).

3. R. J. Hull, S. Marcus, "A Tactical 10.6μm Imaging Radar," Proc. IEEE 1978 NAECON, Dayton, Ohio, May 1978, pp. 662-668.

4. R. H. Kingston, M. Gruber, "Computer Simulation of a Centroid Tracker," private communication (1978).

5. A. Rosenfeld, A. C. Kak, Digital Picture Processing (Academic Press, New York, 1976), pp. 194-195.

6. A. V. Oppenheim, R. W. Schafer, T. G. Stockham, "Nonlinear Filtering of Multiplied and Convolved Signals," Proc. IEEE 56, 1264 (1968).

7. W. K. Pratt, Digital Image Processing (Wiley, New York, 1978), pp. 330-333.

8. T. T. Hwang, "A Well Suited Two-Dimensional Linear Recursive Filter for Image Processing," Proc. IEEE Conf. Acoust., Speech, and Signal Processing, Tulsa, Oklahoma, 10-12 April, 1978.

9. R. A. Hummel, Computer Graphics and Image Processing 6, 184 (1977).

10. R. A. Hummel, Computer Graphics and Image Processing 4, 209 (1975).

11. W. K. Pratt, "Luminance Edge Detection Techniques," USC Semiannual Technical Report (March 1976), pp. 4-21.

12. A. Rosenfeld, A. C. Kak, Digital Picture Processing (Academic Press, New York, 1976) pp. 284-287.

13. G. Robinson, Computer Graphics and Image Processing 6, 492 (1977).

14. J. T. Carlo, J. E. Hall, "Spatial Filtering Using 3 x 3 Kernel Convolutions," Proc. SPIE Technical Symposium East '79 (to be published).

15. R. C. Harney, J. S. Martin, D. R. Sullivan, "Quasi-Three-Dimensional Display of Infrared Radar Images Using Range/Intensity Color Mapping," Technical Note 1978-44, Lincoln Laboratory, M.I.T. (6 December 1978), DDC AD-A070671.

16. D. R. Sullivan, R. C. Harney, J. S. Martin, "Real-Time Quasi-Three-Dimensional Display of Infrared Radar Images," Proc. SPIE Technical Symposium East '79 (to be published).

17. J. S. Lim, H. Nawab, "Restoration of Speckle Images," Technical Note 1979-52, Lincoln Laboratory, M.I.T. (3 July 1979), DDC AD-A074626.

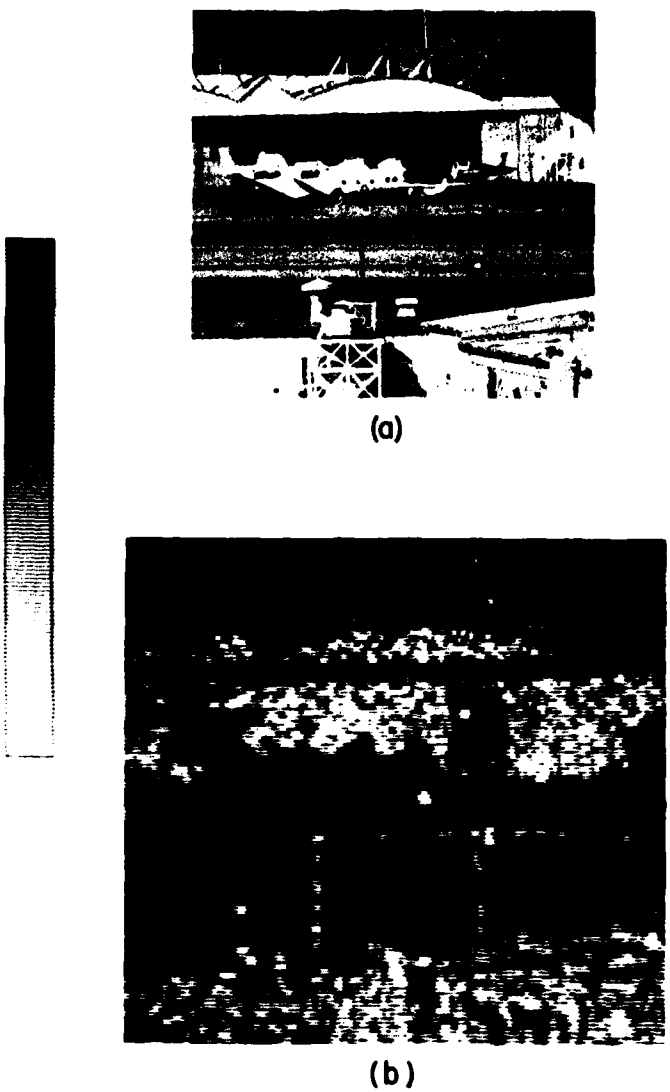

(a)

(b)

Fig. 1(a-b). Lincoln Laboratory Flight Facility (2.7 km) located at Hanscom AFB and foreground: (a) telephoto picture, (b) single frame, intensity-only radar (IRAR) image. Note that the doors of the flight facility were closed at the time that the IR image was recorded.

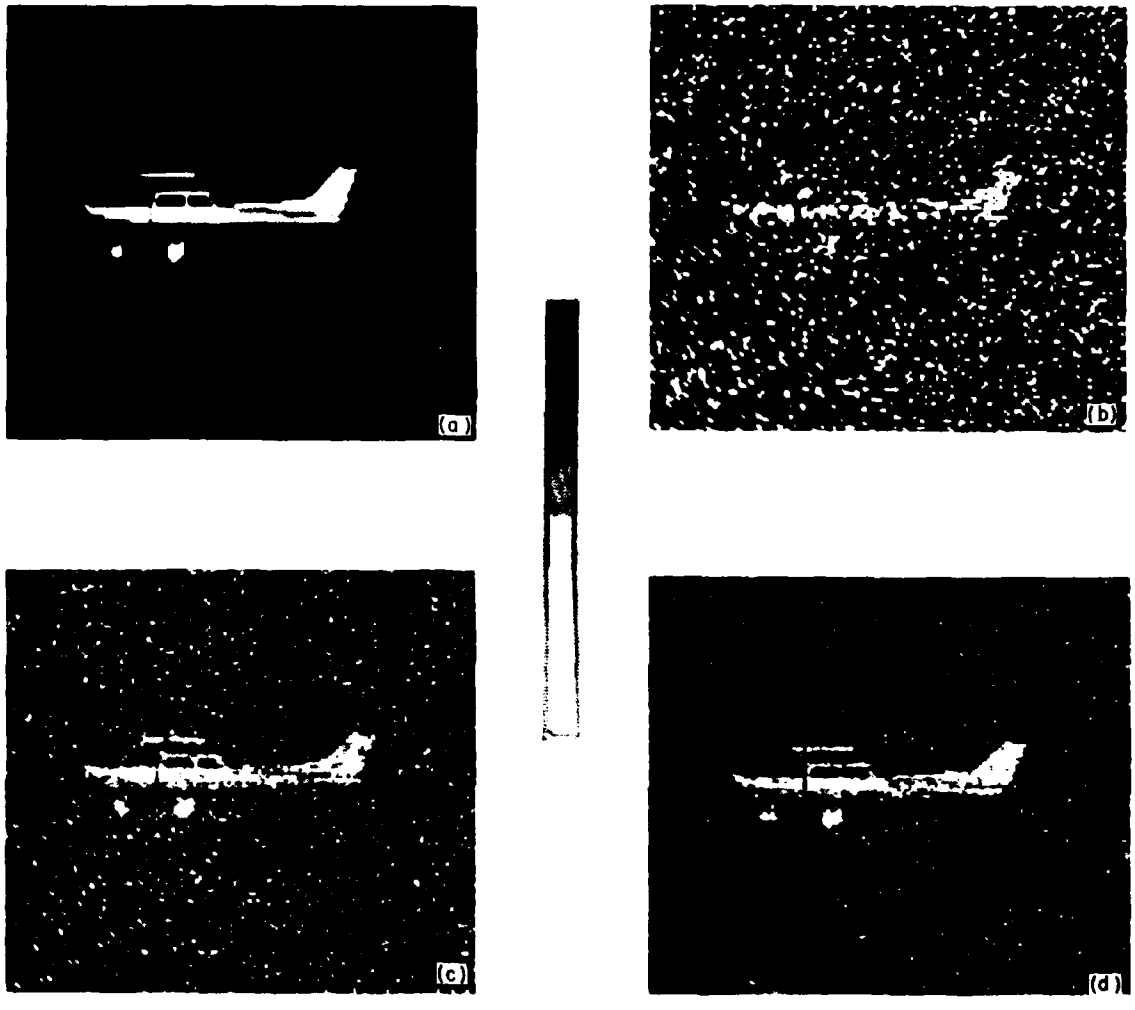


Fig. 2(a-d). Simulation of Cessna aircraft on the ground: (a) Cessna showing relative reflectivity without speckle, (b) after embedding the Cessna into a Gaussian background, the entire scene is speckled (negative exponential), (c) four frame average of the scene, (d) eight frame average of the scene.

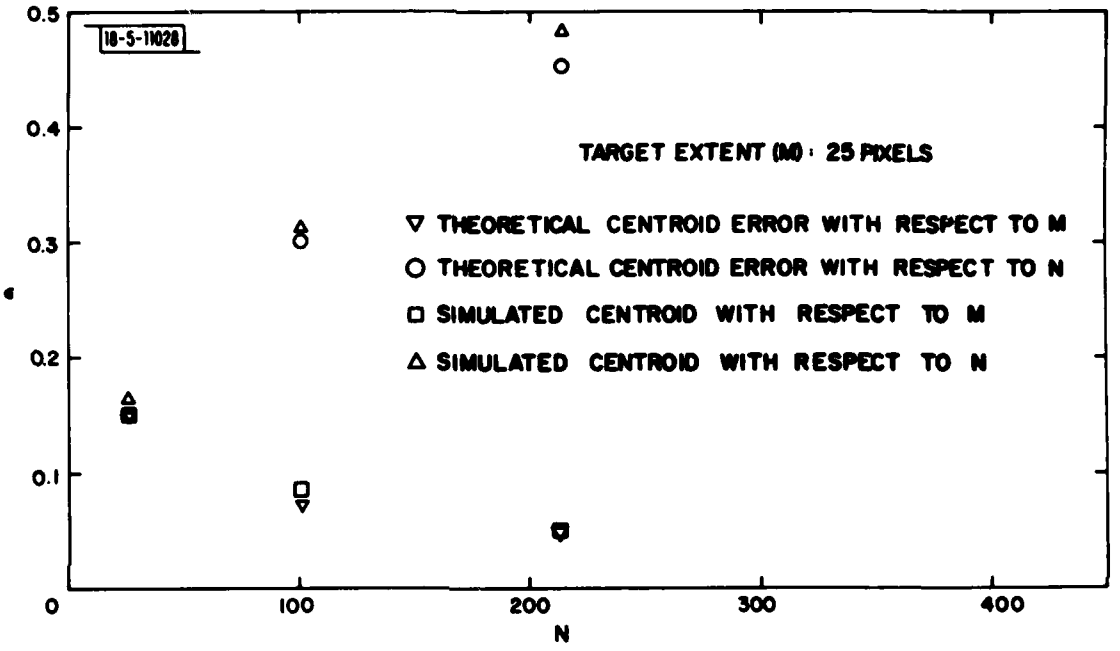


Fig. 3. The RMS error, $\varepsilon$, using a centroid tracker on two hundred statistically independent, Rayleigh speckled data frames generated through simulation. The rectangular target of dimension M x M, is embedded into a background of "zeros" and M is fixed (M = 25).

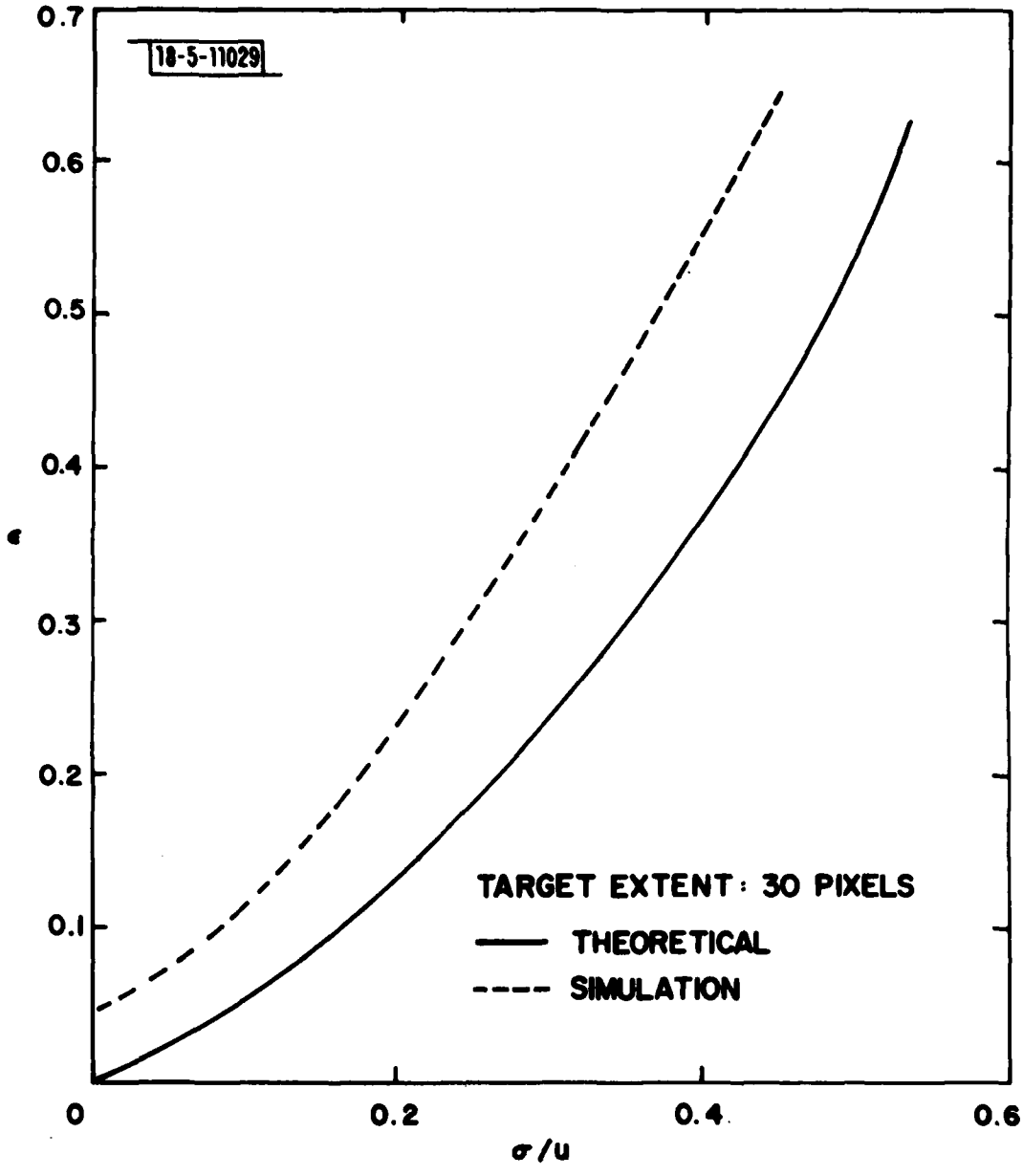


Fig. 4. Theoretical values of the RMS error, $\varepsilon$ (solid line), versus the results of simulation (dashed line) for tracking using cross correlation.

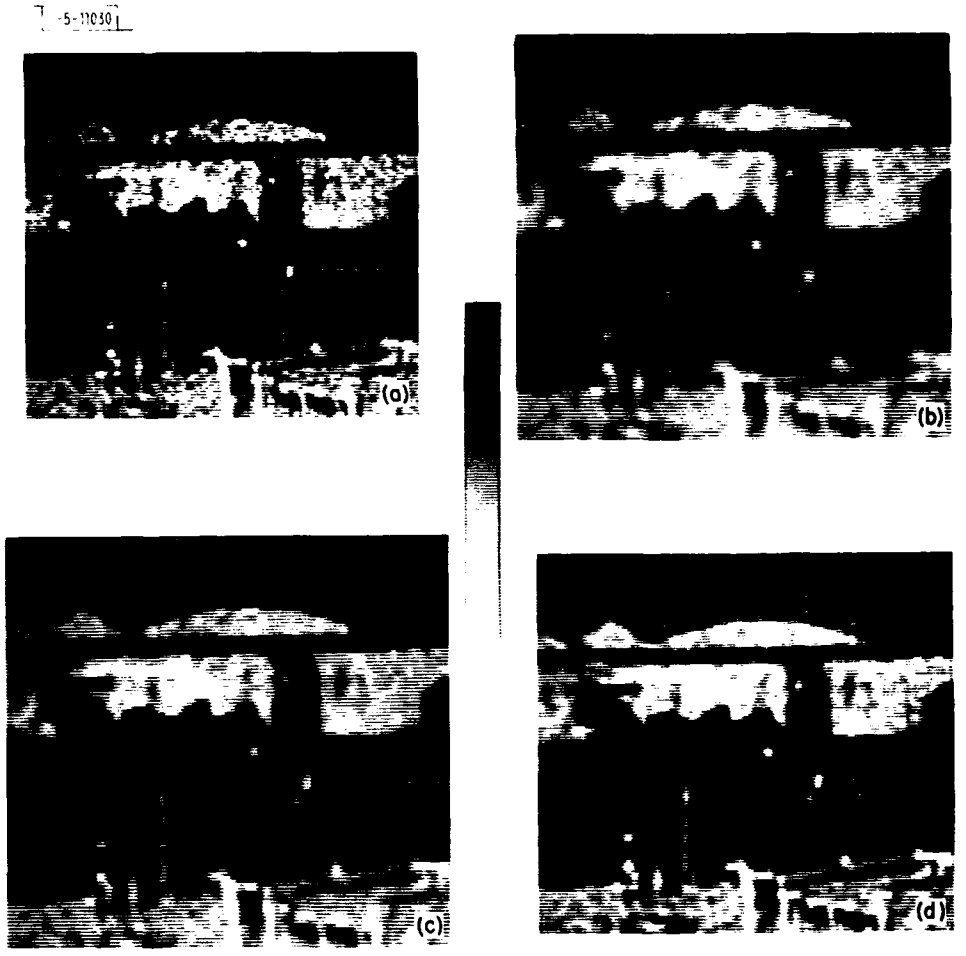


Fig. 5(a-d). Lincoln Laboratory Flight Facility (2.7 km) and fore-ground: (a) intensity-only, eight frame average image of IRAR data, (b) intensity-only, eight frame average, low pass filtered image (moving average filter of dimension 3 x 3), (c) intensity-only, eight frame average, low pass filtered image (separable median filter of dimension 3), (d) intensity-only, eight frame average, low pass filtered image using a homomorphic filter.

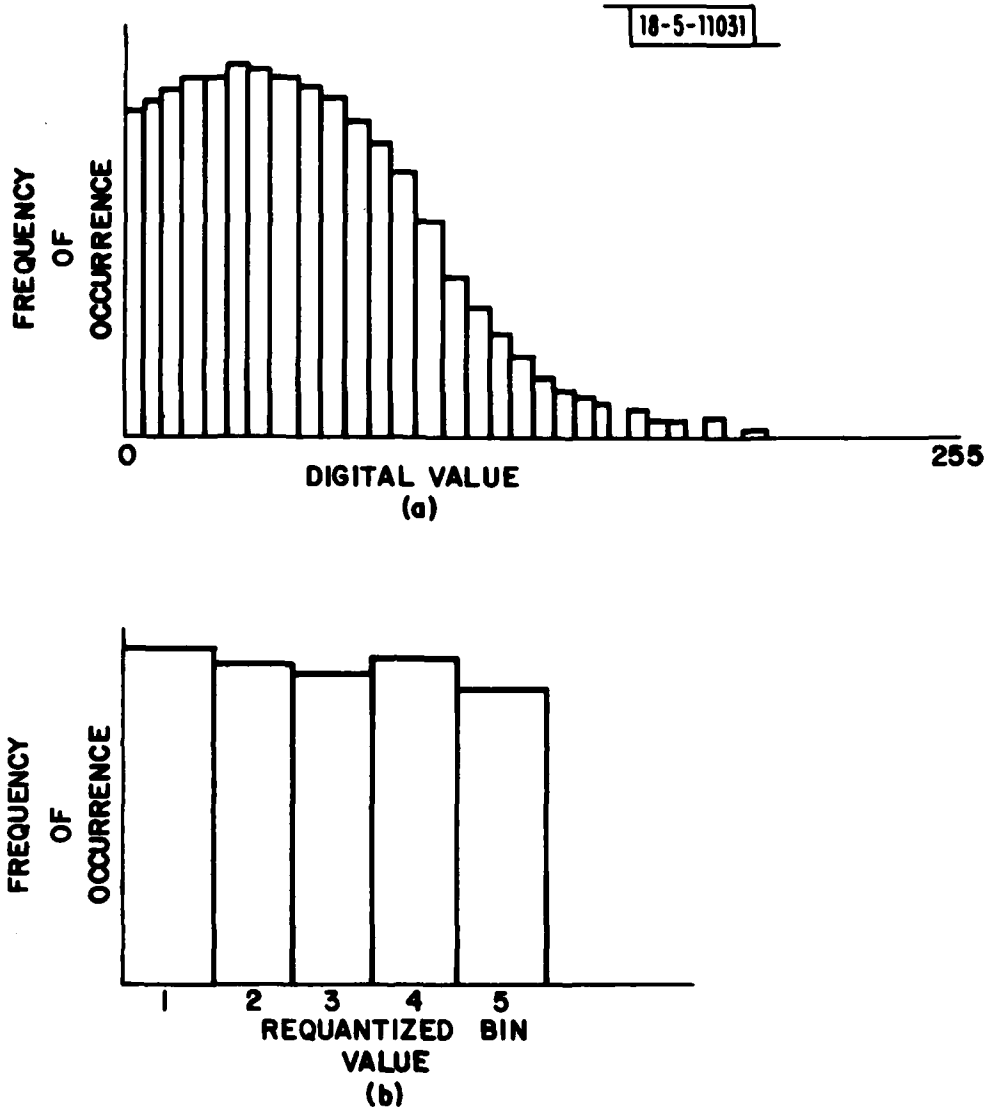


Fig. 6. Histogram equalization.

-5-11032

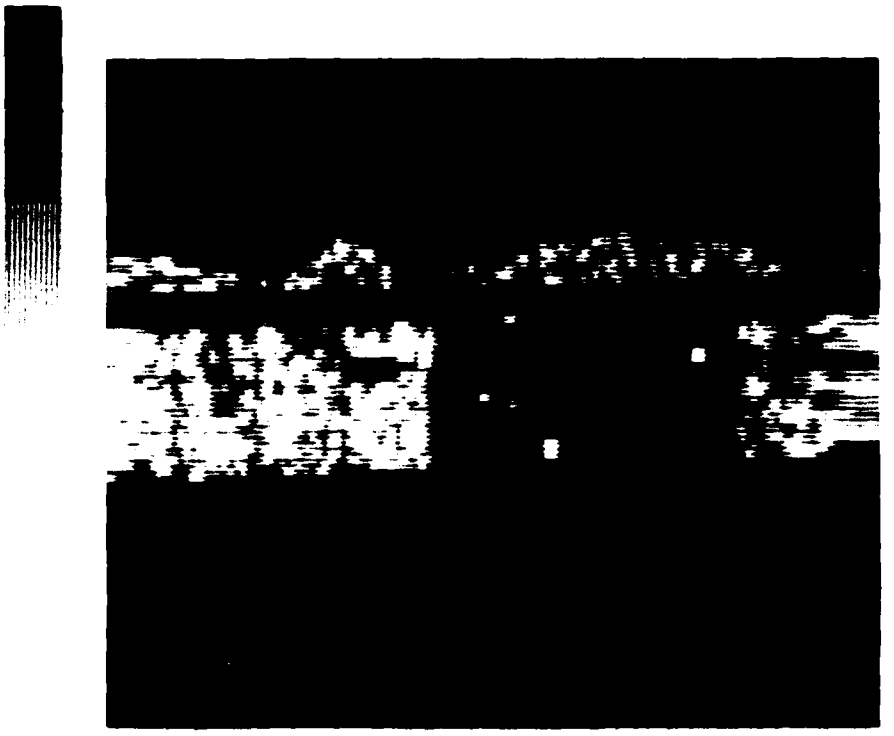

Fig. 7. IRAR histogram equalization. An eight frame average, intensity-only image is requantized into 32 equiprobable bins which are in turn mapped exponentially into the display dynamic range.

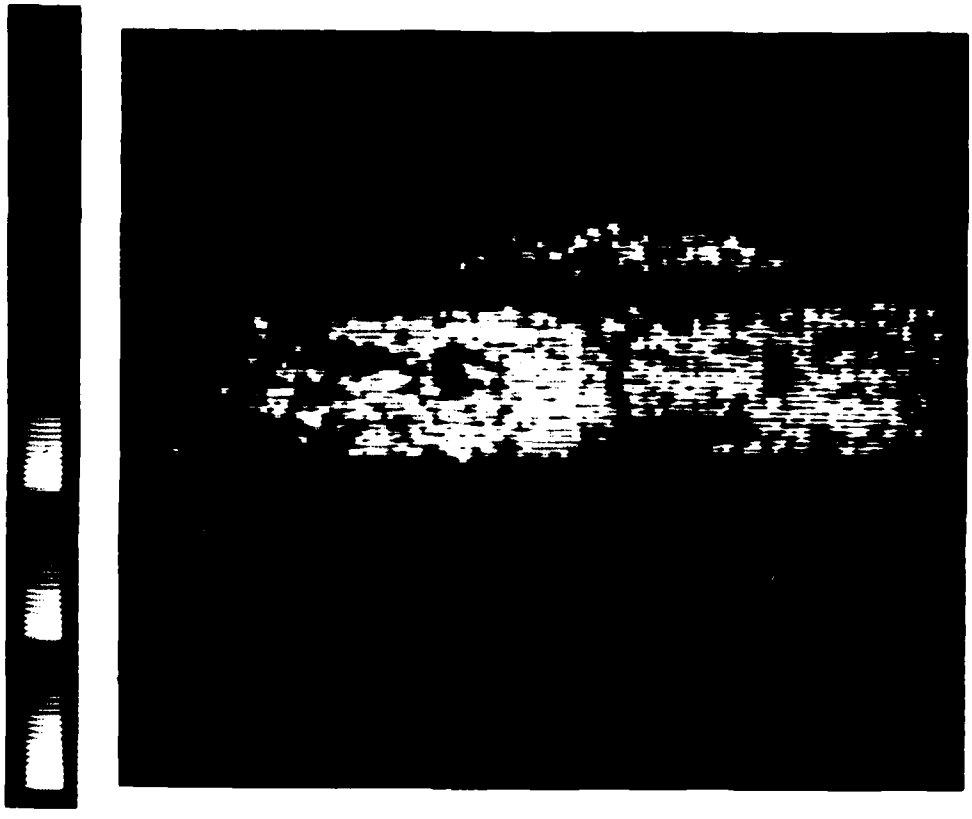

Fig. 8. IRAR histogram equalization using pseudocolor. An eight frame average, intensity-only image is requantized as in Fig. 7, but displayed through a pre-selected video look-up table shown in the color wedge.

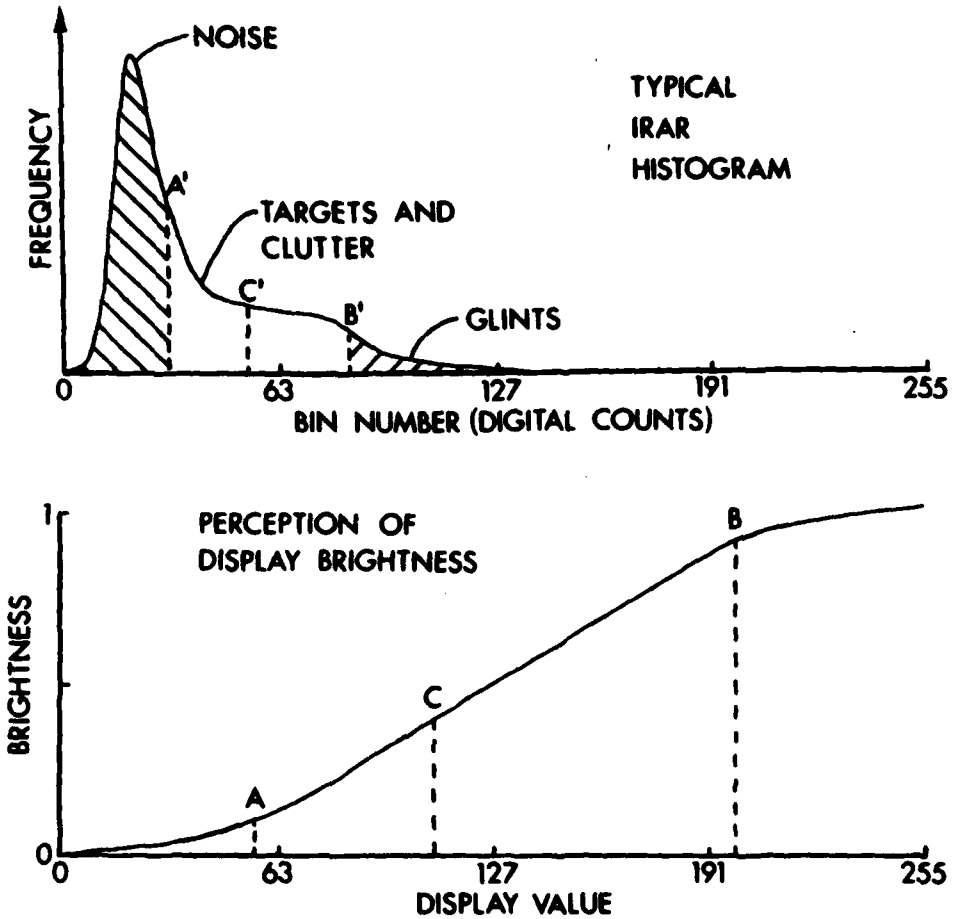


Fig. 9. IRAR automatic gain control procedure.

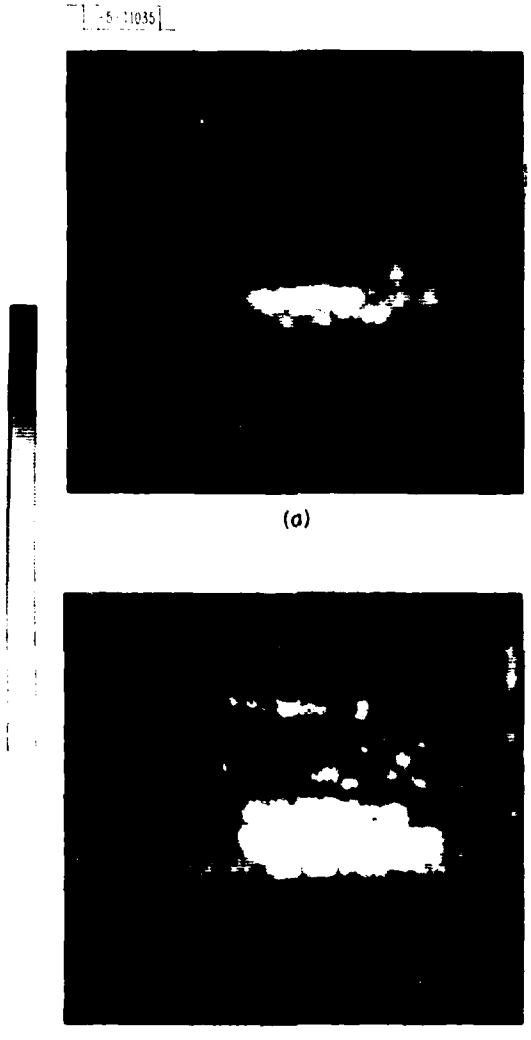

(a)

(b)

Fig. 10(a-b). Canvas covered truck (2.7 km): (a) intensity-only, eight frame average image, (b) intensity-only, eight frame average, image enhanced through the use of IRAR automatic gain control.

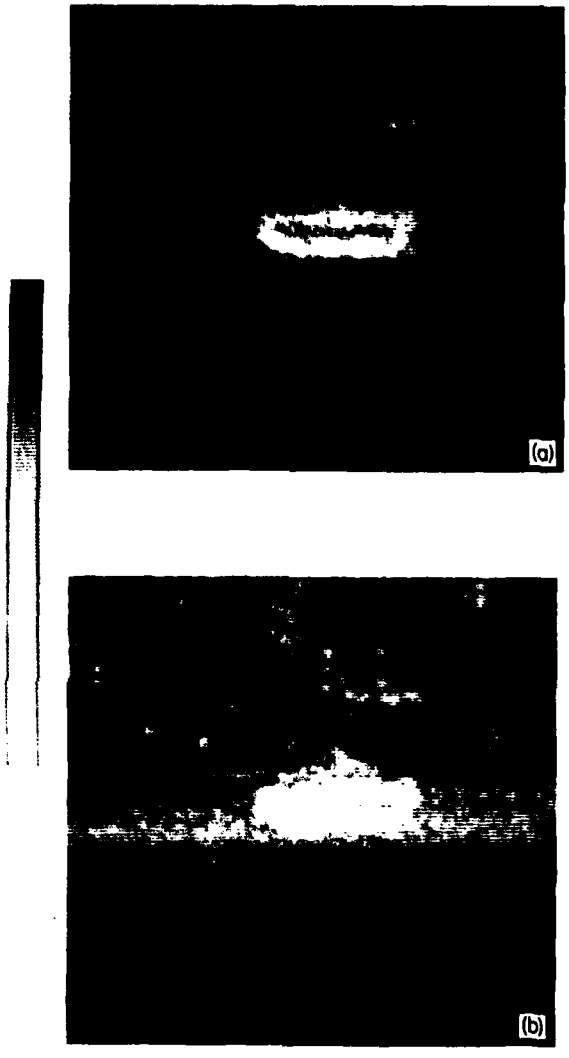


Fig. 11(a-b). U.S. M-60 tank (2.7 km): (a) intensity-only, eight frame average image, (b) intensity-only, eight frame average image enhanced through the use of IRAR automatic gain control.

-5-11037

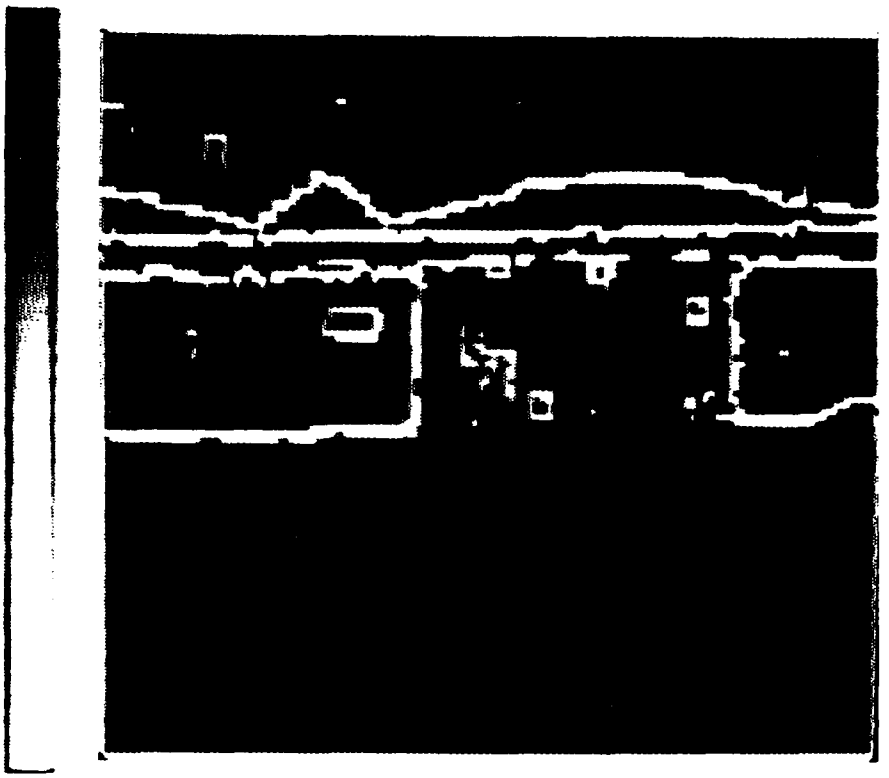

Fig. 12. Lincoln Laboratory flight facility (2.7 km). Intensity-only four frame average, median filtered, then passed through an edge detector.

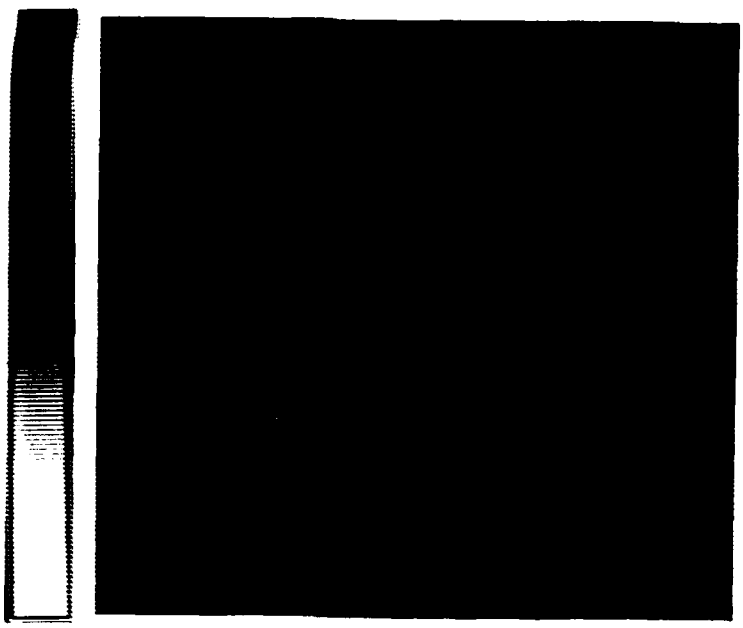

(a)

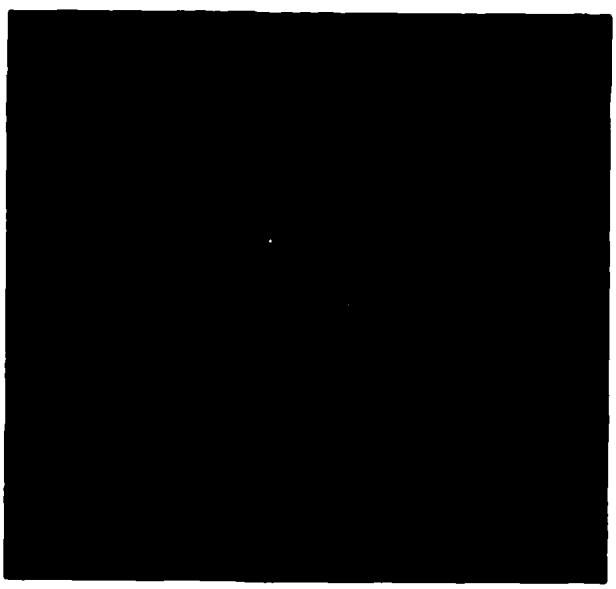

(b)

Fig. 13(a-b). Comparison of same scene viewed in black and white (a) and pseudocolor (b).

Fig. 14. Range/intensity color mapping using five hues (H), each of which has six brightness levels (N).

UNCLASSIFIED

SECURITY CLASSIFICATION OF THIS PAGE *(When Data Entered)*

| REPORT DOCUMENTATION PAGE | READ INSTRUCTIONS BEFORE COMPLETING FORM |
|---|---|
| 1. REPORT NUMBER: ESD-TR-79-271 | 2. GOVT ACCESSION NO. / 3. RECIPIENT'S CATALOG NUMBER |
| 4. TITLE *(and Subtitle)*: IRAR Image Processing Techniques | 5. TYPE OF REPORT & PERIOD COVERED: Project Report |
| | 6. PERFORMING ORG. REPORT NUMBER: Project Report TST-41 |
| 7. AUTHOR(s): Dorothy R. Sullivan | 8. CONTRACT OR GRANT NUMBER(s): F19628-80-C-0002 |
| 9. PERFORMING ORGANIZATION NAME AND ADDRESS: Lincoln Laboratory, M.I.T.<br>P.O. Box 73<br>Lexington, MA 02173 | 10. PROGRAM ELEMENT, PROJECT, TASK AREA & WORK UNIT NUMBERS: Program Element No. 63250F<br>Project No. 649L |
| 11. CONTROLLING OFFICE NAME AND ADDRESS: Air Force Systems Command, USAF<br>Andrews AFB<br>Washington, DC 20331 | 12. REPORT DATE: 7 November 1979<br>13. NUMBER OF PAGES: 50 |
| 14. MONITORING AGENCY NAME & ADDRESS *(if different from Controlling Office)*: Electronic Systems Division<br>Hanscom AFB<br>Bedford, MA 01731 | 15. SECURITY CLASS. *(of this report)*: Unclassified<br>15a. DECLASSIFICATION DOWNGRADING SCHEDULE |

16. DISTRIBUTION STATEMENT *(of this Report)*

Approved for public release; distribution unlimited.

16 649L

17. DISTRIBUTION STATEMENT *(of the abstract entered in Block 20, if different from Report)*

14 TST-41

18. SUPPLEMENTARY NOTES

None

19. KEY WORDS *(Continue on reverse side if necessary and identify by block number)*

| | | |
|---|---|---|
| contrast manipulation | image enhancement | low pass filter |
| edge detection | image registration | range/intensity color mapping |
| IRAR | infrared radar | speckle |

20. ABSTRACT *(Continue on reverse side if necessary and identify by block number)*

This report examines the problems associated with the display of active (10.6 μm) infrared radar images. Issues addressed include degradations introduced by the imaging sensor, the effects of these degradations on image tracking and image enhancement, and evaluation of various tracking and enhancement techniques in view of their usefulness and potential hardware implementation. The performance of each algorithm is demonstrated using either simulated data or data collected by the Infrared Airborne Radar (IRAR) testbed system.

DD FORM 1 JAN 73 1473 EDITION OF 1 NOV 65 IS OBSOLETE

UNCLASSIFIED

SECURITY CLASSIFICATION OF THIS PAGE *(When Data Entered)*